Lyα imaging around the hyperluminous dust-obscured quasar W2246−0526 at $z = 4.6$

Yibin Luo （罗毅彬） [ID],[1,2] Lulu Fan （范璐璐） [ID],[1,2,3] Yongming Liang （梁永明） [ID],[4] Weida Hu （胡维达） [ID],[5,6]
Junxian Wang （王俊贤） [ID],[1,2] Zhen-ya Zheng （郑振亚） [ID],[7] Zheyu Lin （林哲宇） [ID],[1,2] Bojun Tao （陶柏钧） ,[1,2]
Zesen Lin （林泽森） [ID],[8] minxuan Cai,[1,2] mengqiu Huang （黄梦秋） [ID],[1,2] Zhen Wan （宛振） [ID],[1,2] and
Yongling Tang （唐永灵） [1,2]

[1]CAS Key Laboratory for Research in Galaxies and Cosmology, Department of Astronomy, University of Science and Technology of
China, Hefei 230026, China
[2]School of Astronomy and Space Science, University of Science and Technology of China, Hefei 230026, China
[3]Deep Space Exploration Laboratory, Hefei 230088, China
[4]Institute for Cosmic Ray Research, The University of Tokyo, 5-1-5 Kashiwanoha, Kashiwa, Chiba 277-8582, Japan
[5]Department of Physics and Astronomy, Texas A&M University, College Station, TX, 77843-4242 USA
[6]George P. and Cynthia Woods Mitchell Institute for Fundamental Physics and Astronomy, Texas A&M University, College Station, TX,
77843-4242 USA
[7]CAS Key Laboratory for Research in Galaxies and Cosmology, Shanghai Astronomical Observatory, Shanghai 200030, China
[8]Department of Physics, The Chinese University of Hong Kong, Shatin, N.T., Hong Kong S.A.R., China

ABSTRACT

Hot dust-obscured galaxies (Hot DOGs) are a population of hyperluminous, heavily obscured quasars discovered by the *Wide-field Infrared Survey Explorer* (*WISE*) all-sky survey at high redshift. Observations suggested the growth of these galaxies may be driven by mergers. Previous environmental studies have statistically shown Hot DOGs may reside in dense regions. Here we use the Very Large Telescope (VLT) narrowband and broadband imaging to search for Lyα emitters (LAEs) in the $6.8' \times 6.8'$ field of the Hot DOG W2246−0526 at $z = 4.6$. W2246−0526 is the most distant Hot DOG. We find that there is an overdensity of LAEs in W2246−0526 field compared with the blank fields. This is the direct evidence that this most distant Hot DOG is in an overdense environment on the Mpc scale, and the result relates to the merger origin of Hot DOGs.

Keywords: galaxies: active galaxies: formation - galaxies: evolution - galaxies: high redshift - galaxies: clusters

1. INTRODUCTION

Based on "W1W2-dropout" method, a new population of hyperluminous, hot dust-obscured galaxies were discovered using the WISE and were called as Hot DOGs (Eisenhardt et al. 2012; Wu et al. 2012). These galaxies are prominent in the WISE 12 μm (W3) and 22 μm (W4) bands, but are very faint or undetected in the 3.4 μm (W1) and 4.6 μm (W2) bands. Previous studies have found that Hot DOGs are extremely luminous $L_{bol} > 10^{13} L_{\odot}$, heavily dust-obscured quasars at high redshift, and represent a transition phase between starburst-dominated phase and optically bright quasars

phase (Assef et al. 2015; Fan et al. 2016a, 2018, 2020; Piconcelli et al. 2015; Stern et al. 2014; Sun et al. 2024; Fernández Aranda et al. 2024).

Models predict that the growth of these galaxies may be driven by mergers (Hopkins et al. 2006; Di Matteo et al. 2008). Galaxy mergers remove gas angular momentum and drive it directly into the center, fueling intense starbursts and central SMBH accretion. Multiwavelength observations of Hot DOGs also suggested that Hot DOGs are likely triggered by galaxy mergers. Fan et al. (2016b) found a high merger fraction ($62 \pm 14\%$) in a sample of 18 Hot DOGs using Hubble Space Telescope (HST) WFC3 imaging. Atacama Large Millimeter Array (ALMA) observations of a sample of 7 Hot DOGs suggested that there may be multiple merger events at the stage of Hot DOGs (Diaz-Santos et al. 2021). High merger fraction may be associated

Corresponding author: Yibin Luo,Lulu Fan
yibinluo@mail.ustc.edu.cn,llfan@ustc.edu.cn

with high-density regions. Although some statistical studies have found overdensities of mid-IR-selected and sub-millimeter-selected galaxies around Hot DOGs (Assef et al. 2015; Jones et al. 2014, 2017; Fan et al. 2017), and two case studies have found overdensities of distant red galaxies (DRGs) (Luo et al. 2022) and Lyman Break Galaxies (LBGs) (Zewdie et al. 2023) around Hot DOGs, direct observations such as spectroscopically confirmed companion galaxies or narrowband observations are still very rare. Ginolfi et al. (2022) found an overdensity of Lyman-alpha emitters (LAEs) around a $z = 3.6$ Hot DOG using the VLT/MUSE. Diaz-Santos et al. (2018) found a $z = 4.6$ Hot DOG (W2246$-$0526, which is the most distant Hot DOG) in a multiple merger system using ALMA observations, with at least three spectroscopically confirmed companion galaxies within a few tens of kpc. Due to the limitations of the field of view of ALMA, the study of environment was restricted to scales of a few tens of kpc. Considering previous environment studies suggested that Hot DOGs may be a good tracer for overdense regions such as protoclusters, it is important to further study the environments of Hot DOGs in clusters scales of Mpc.

A commonly used technique to identify high-redshift galaxies is to search for sources with a prominent Lyα emission using specific narrowband filters ($\Delta\lambda \sim 100$Å). These sources are called as Lyα emitters (LAEs). The covered redshift range of this technique is narrow ($\Delta z \sim 0.1$), which can reduce the impact of projection effects on environment studies. Numerous studies have used this technique to study the large scale environment (Venemans et al. 2002, 2005, 2007; Cai et al. 2017; Mazzucchelli et al. 2017; Kikuta et al. 2017; Zheng et al. 2017; García-Vergara et al. 2019; Hu et al. 2019; Liang et al. 2021; Hu et al. 2021).

In this work, we use narrowband and broadband images obtained from VLT FOcal Reducer and low dispersion Spectrograph 2 (FORS2, Appenzeller & Rupprecht 1992) to study the environment of the Hot DOG W2246$-$0526 (hereafter, W2246) by searching LAEs in this field. The redshift of W2246 derived from ALMA [CII] line is $z = 4.601$ (Diaz-Santos et al. 2016). Among the Hot DOGs with spectroscopic redshift, W2246 is the most distant one so far. In addition, W2246 is the most luminous one with bolometric luminosity $L_{bol} > 10^{14}L_{\odot}$ (Tsai et al. 2015). Strong AGN feedback was found in W2246 (Diaz-Santos et al. 2016). Fan et al. (2018) found that most of its IR luminosity come from AGN torus, suggesting the rapid growth of the central SMBH. Tsai et al. (2018) measured the SMBH mass of about $10^{10}M_{\odot}$, and the Eddington ratio of 2.8.

The paper is structured as follows. We present the observation and data reduction in Section 2. We describe the color criteria and LAE sample in Section 3. Results and discussions are described in Section 4 and Section 5, respectively. Finally, we give the summary and conclusion in Section 6. Throughout this work, we use the AB magnitude system and assume a cosmology with $H_0 = 70$ km s^{-1} Mpc^{-1}, $\Omega_M = 0.27$ and $\Omega_\Lambda = 0.73$ (Komatsu et al. 2011). All magnitudes are corrected for Galactic extinction (Schlafly & Finkbeiner 2011).

2. OBSERVATION AND DATA REDUCTION

We obtained narrowband and broadband imaging of the W2246 field with the FORS2 at the VLT in 2017 June and July. We used the red sensitive detector consisting of two 2k×4k MIT CCDs and adopted a 2×2 binning readout mode. The pixel scale is $0''.25$/pixel, and the field of view (FOV) of FORS2 is 6.8×6.8 arcmin^2, corresponding to 15.45×15.45 cMpc^2 at $z = 4.6$. Here cMpc is the abbreviation of comoving Mpc. The field was observed in the narrowband filter SII/2000+63 ($\lambda_c = 6774$Å, FWHM = 68Å, hereafter NB) and the broadband filters R_SPECIAL ($\lambda_c = 6550$Å, FWHM = 1650Å, hereafter R) and V_HIGH ($\lambda_c = 5550$Å, FWHM = 1232Å, hereafter V). The total exposure times for NB, R, and V bands are about 5.3, 1.0 and 1.5 hours, respectively.

We processed the standard data reduction techniques using the ESO's EsoRex pipeline (Freudling et al. 2013). We used the fors_bias, fors_img_sky_flat, and fors_img_science pipeline recipes from EsoRex to perform bias subtraction and flat fielding. Considering that the W2246 field has several bright stars, especially two heavily saturated bright stars, we used PHOTUTILS package in PYTHON to do the background subtraction. For the photometric calibration of the R, and V bands images, the Stetson photometric fields (Stetson 2000) were observed in these bands. The Stetson photometric standard stars catalog was used for the calibration of the R, and V bands images. The process was done using fors_zeropoint and fors_photometry pipeline recipes from EsoRex. Spectrophotometric standard stars (Turnshek et al. 1990; Hamuy et al. 1992, 1994) were observed in NB to calibrate the narrowband images. We used PYPHOT[1] to perform the photometric calibration. The calibrated frames are stacked to generate a deeper image for each band by using SWARP (Bertin et al. 2002). The FWHMs of the point spread function (PSF) are $1''.39$, $1''.21$, and $0''.97$ in the NB, R,
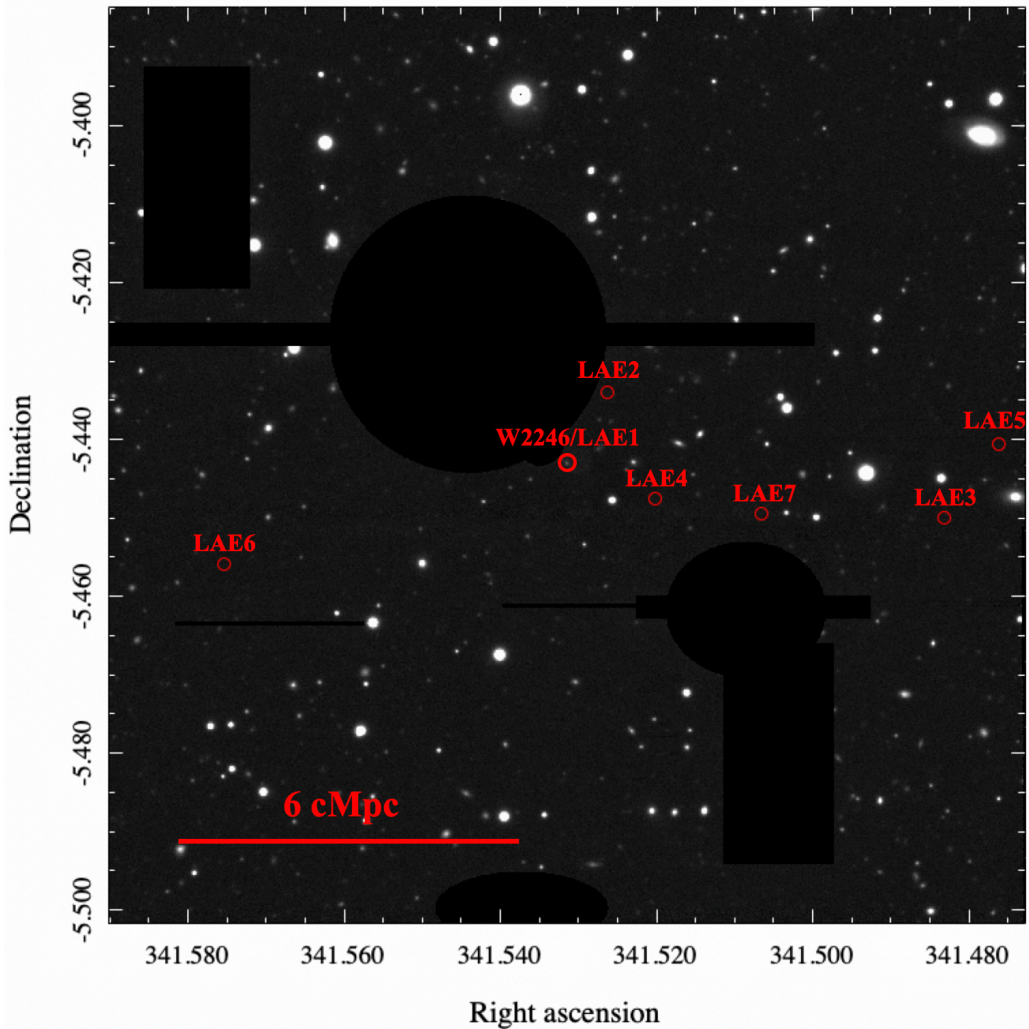
---

[1] https://mfouesneau.github.io/pyphot/index.html

Figure 1. NB image of the W2246 field and the effective area is 33.6 arcmin^2. Positions of the LAEs are shown using the red circle and the bold red circle marks the position of W2246.

and V bands, respectively. In order to measure the colors within the same aperture, we match the PSF of the R and V bands images to the NB image (the one with the worst PSF) using PHOTUTILS. Photometry was performed using SExtractor (Bertin & Arnouts 1996) in dual-image mode with the NB image as the detection image. We use 2″5 diameter aperture magnitudes for the color measurements. The 5σ limiting magnitudes (with 2″5 diameter aperture) of the NB, R, and V bands are 25.5, 26.2, and 26.9 mag, respectively. We adopted AUTO magnitudes as the total magnitude of detected sources. The effective area of the reduced image is 33.6 arcmin^2. Regions that contain saturated bright stars and severe stray light caused by instrument are masked. Figure 1 shows the NB image of the W2246 field. We estimated the detection completeness of the NB image as a function of total NB magnitude. We randomly distributed mock point sources (gaussian profile, FWHM =

1″4) with different magnitude into the effective area of NB image. Then, we ran the SExtractor with the same detection parameters, and checked whether the added source was detected or not. The results are shown in Figure 2. The detection completeness drops to about 80 percent at $NB_{tot} = 25.1$ mag.

3. LAES SELECTION

3.1. *Selection Criteria*

We use color selection criteria to select LAEs from photometric catalog, which is commonly used in previous studies (Venemans et al. 2002, 2005; Ouchi et al. 2008; Mazzucchelli et al. 2017; García-Vergara et al. 2019; Hu et al. 2019; Liang et al. 2021). To define the selection criteria, we assume that the LAE model spectrum at $z \sim 4.6$ has a Gaussian profile Lyα emission with a power-law UV continuum ($f_\lambda \propto \lambda^\beta$). The LAE model spectrum are corrected for the IGM absorp-
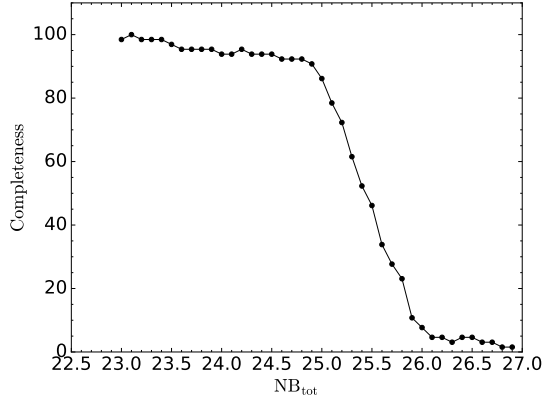
Figure 2. The detection completeness of the NB image as a function of NB_{tot} magnitude. The detection completeness drops to about 80 percent at $NB_{tot} = 25.1$ mag.
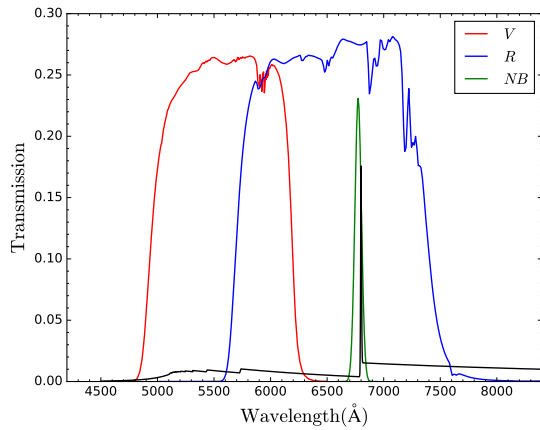

Figure 3. Total transmission curves of NB, R, and V filters, including the instrument response and atmospheric transmission at airmass of 1.2. The LAE model spectrum corresponds to a galaxy with UV continuum slope $\beta = -2$ and rest frame Lyα equivalent width $EW_0 = 20$ Å. Redshift of this model spectrum is $z = 4.6$. The LAE model spectrum are corrected for the IGM absorption (Inoue et al. 2014).

tion with the model from Inoue et al. (2014). Then, we convolve the model spectrum with filters total transmission curves (including the instrument response and atmospheric transmission) to calculate the magnitude in each filter. Finally, the color excess can be estimated from this simulation. The total transmission curves of three filters and the LAE model spectrum are shown in Figure 3. We consider the Lyα emission of model spectrum has a rest equivalent width $EW_0 = 20$ Å, which is the conventional value to define LAEs (Ouchi et al. 2020). The predicted track of LAE model from redshift 3.8 to 5.2 is plotted in the color-color diagram in the left panel of Figure 4. Different UV continuum slopes β from -3 to -1 are set in the simulation and are shown

in the right panel of Figure 4. We find that when UV continuum slopes β changes, it mainly affects the color of $V - R$, and has little effect on the color of $R - NB$. We also consider possible contaminants such as low redshift [OII] emitters, [OIII] emitters, elliptical galaxies, and spiral galaxies (Sa, Sb, Sc) in our estimation of the color selection criteria. The number densities of [OII] and [OIII] emitters at low redshift had been studied in Pirzkal et al. (2013). Following the calculation of Zheng et al. (2013), we estimate the number of [OII] and [OIII] emitters are 0.03 and 0.04 in the W2246 field, which has little impact on our LAEs selection. For the elliptical galaxies and spiral galaxies, we get these galaxies templates from the SWIRE library (Polletta et al. 2007). The predicted tracks of the elliptical galaxies and spiral galaxies from redshift 0 to 3 are also plotted in the left panel of Figure 4. From the color-color diagram, we can find that although $R - NB = 0.5$ mag at $z = 4.601$ is smaller than the peak of $R - NB$ of LAE model, which is due to the central wavelengths of the narrow-band filter shifts from the W2246 redshift derived from ALMA. We call this phenomenon as the shift of the observation window. However, the $R - NB$ of LAE at $z = 4.601$ is still significant larger than the $R - NB$ of elliptical and spiral galaxies. In addition, the $V - R$ of LAE model is about 0.4 when UV continuum slopes β down to -3. Considering the contamination of low-redshift [OII] and [OIII] emitters in our study is negligible, we use this value in the $V - R$ color criterion. Therefore, we select LAE using the following criteria:

$$
\begin{aligned}
& R - NB > 0.5, \\
& V - R > 0.4, \\
& R - NB > 2 \times \sqrt{\sigma_R^2 + \sigma_{NB}^2}, \\
& 20 < NB < NB_{lim,4\sigma},
\end{aligned}
\tag{1}
$$

We set the 2σ significant of the narrow-band excess criterion to avoid contamination by sources that satisfy the color criteria only due to photometric errors. The lower limit for the NB magnitude is to avoid saturation, and the upper limit is to search for more faint LAEs while ensuring high reliability.

3.2. *LAE Sample*

For sources in the photometric catalog generated by SExtractor, we require that sources have the SExtractor parameter FLAGS=0 to discard unreliable sources such as blended, saturated, or truncated sources. We only consider the sources that have $20 < NB < NB_{lim,4\sigma}$ in the NB image. We adopt a 2σ limiting magnitudes in R and V bands for marginal detections in the broadband images. In order to rule out possi-

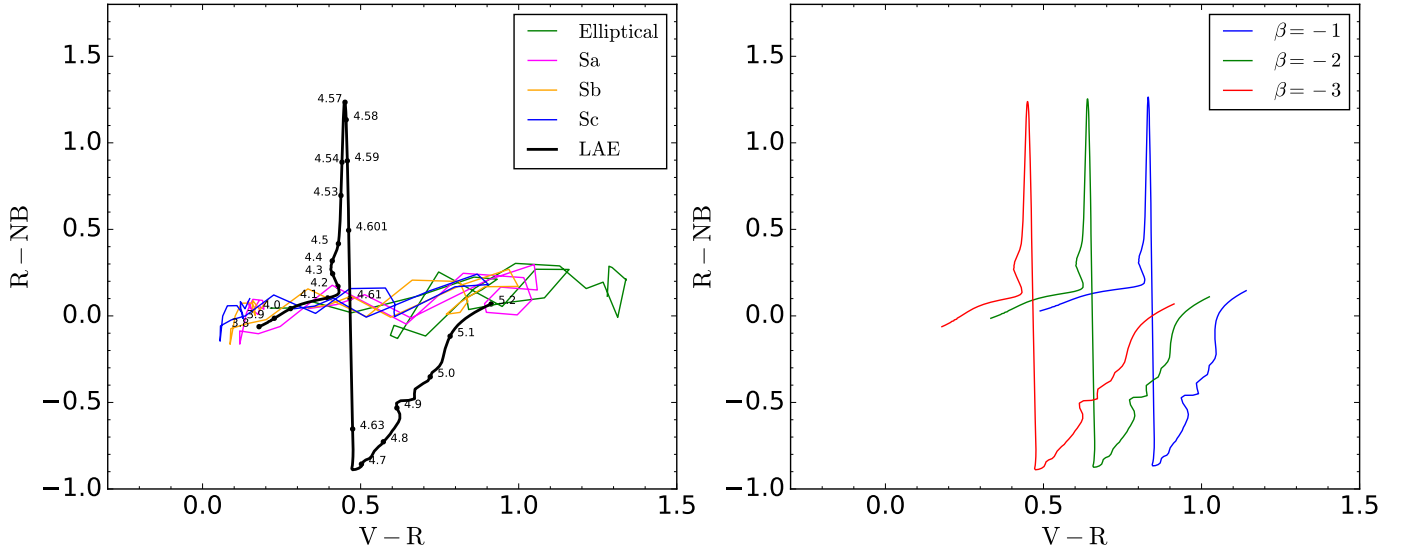**Figure 4.** Left: evolutionary track of an LAE with $EW_0 = 20$ Å(black curve). Points over the black curve indicate colors of LAEs from redshift 3.8 to 5.2, and the redshift of W2246 $z_{[CII]} = 4.601$ is also shown. We also plotted the evolutionary tracks of possible contaminants redshifted from 0 to 3. Green, magenta, orange, and blue curves are the evolutionary track of elliptical, Sa, Sb, and Sc galaxies, respectively. Right: we show the evolutionary track of LAE model spectrum with three different UV slopes, ranging from $\beta = -3$ to $\beta = -1$.

ble spurious sources, we require the sources have $\geq 2\sigma$ detection in at least one broadband image. We show the $R - NB$ and $V - R$ color-color diagram of all the sources that satisfy the above conditions in Figure 5. There are seven sources that satisfy our LAE selection criteria and are considered to be LAE candidates. We show their postage stamps in NB, R, and V bands in Figure 6. Six of the seven sources are detected in all three bands, only one source are detected in NB and R bands but not detected in the V band. Among these LAE candidates, the Hot DOG W2246 itself is selected to be a LAE candidate. Considering W2246 was spectroscopically confirmed to be a LAE in Diaz-Santos et al. (2021), W2246 is selected by the criterion is an expected result, and indicate the parameters for our criteria are appropriate.

4. RESULTS

4.1. *Photometric Properties of the LAEs*

We calculate the Lyα line luminosity of LAE candidates from the photometry using the formulas from Venemans et al. (2005):

$$F_{Ly\alpha} = \frac{\Delta\lambda_R \Delta\lambda_{NB}(f_{\lambda,NB} - f_{\lambda,R})}{\Delta\lambda_R - \Delta\lambda_{NB}},$$

$$L_{Ly\alpha} = 4\pi d_L^2 F_{Ly\alpha}, \tag{2}$$

In the formulas, $\Delta\lambda_{NB}$ and $\Delta\lambda_R$ are the FWHM of NB and R filters, $f_{\lambda,NB}$ and $f_{\lambda,R}$ are the flux density in the NB and R filters, d_L is the luminosity distance. We also estimate Star Formation Rate (SFR) use the following empirical relation between SFR and $L_{Ly\alpha}$ (Ouchi et al. 2008). The Lyα luminosity and SFR of seven LAE candidates are listed in Table 1.

$$\mathrm{SFR}(M_\odot\ yr^{-1}) = \frac{L_{Ly\alpha}}{1.1 \times 10^{42}\ erg\ s^{-1}} \tag{3}$$

4.2. *Spatial distribution of LAEs*

The spatial distribution of LAEs in the W2246 field is shown in Figure 1. We can intuitively find the concentration of LAEs near Hot DOGs. In order to quantitatively describe this phenomenon, we show the surface density distribution of LAEs as a function of distance to Hot DOG W2246 in Figure 7. The surface density of LAEs in the vicinity of Hot DOGs is higher than that of the whole field. We also find the size of the concentration region is small. When the distance increases to 6 cMpc, the surface density of LAEs rapidly drops to 1/6 of the value at the distance of 2 cMpc. The detail of analyzing the impact of size on environment study is described in Section 4.3 and Section 5. In addition, LAEs in Figure 1 do not seem to be randomly oriented but rather then seem to follow a filamentary-like orientation. The discussion of this phenomenon is described in Section 5.

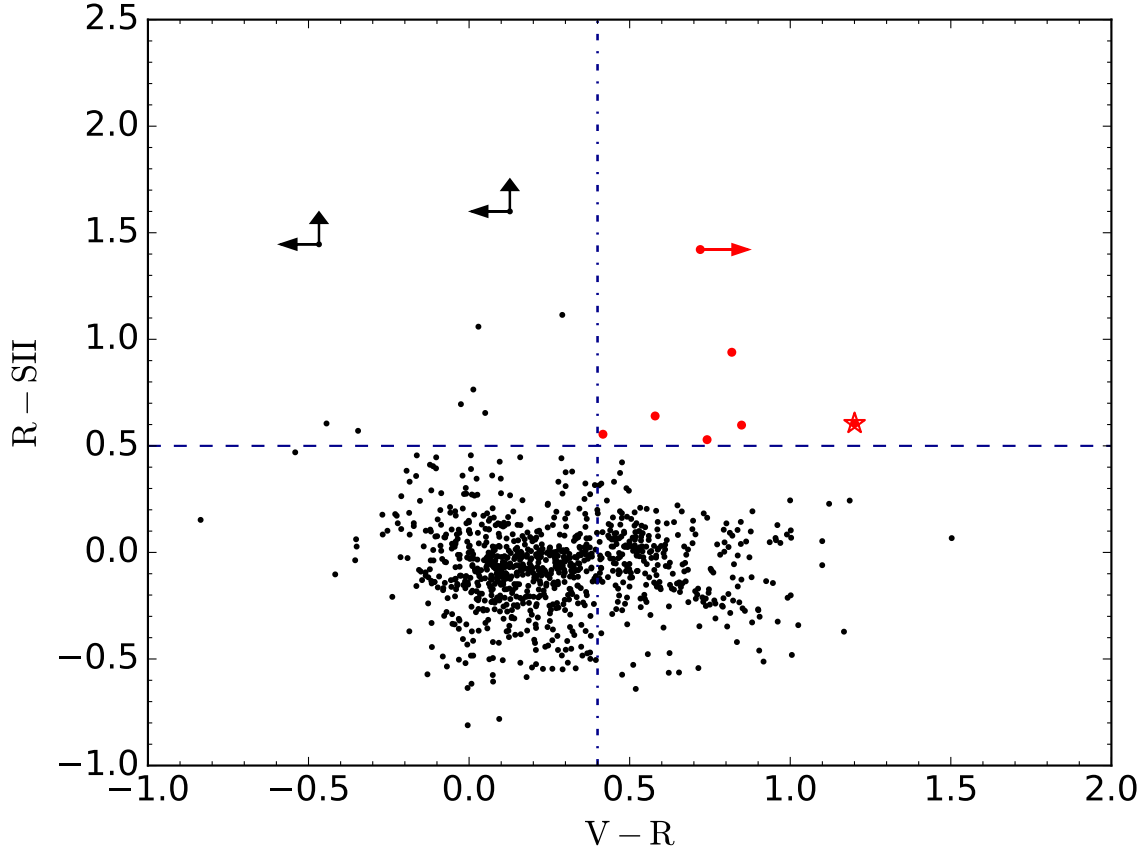### 4.3. *Comparison with the Number Density of LAEs in Blank Fields*

Figure 5. Color-color diagram of the sources in the W2246 field. Horizontal and vertical dashed lines corresponds color criteria $R - NB > 0.5$ and $V - R > 0.4$. Sources selected as LAEs are marked as red filled circles. Red arrow indicates lower limit for the $V - R$ color, in which the source is not detected at the 2σ level in V image. Black arrows indicate sources that are detected under 2σ level in R images. The open star marks the Hot DOG W2246.

Table 1. Photometric Properties

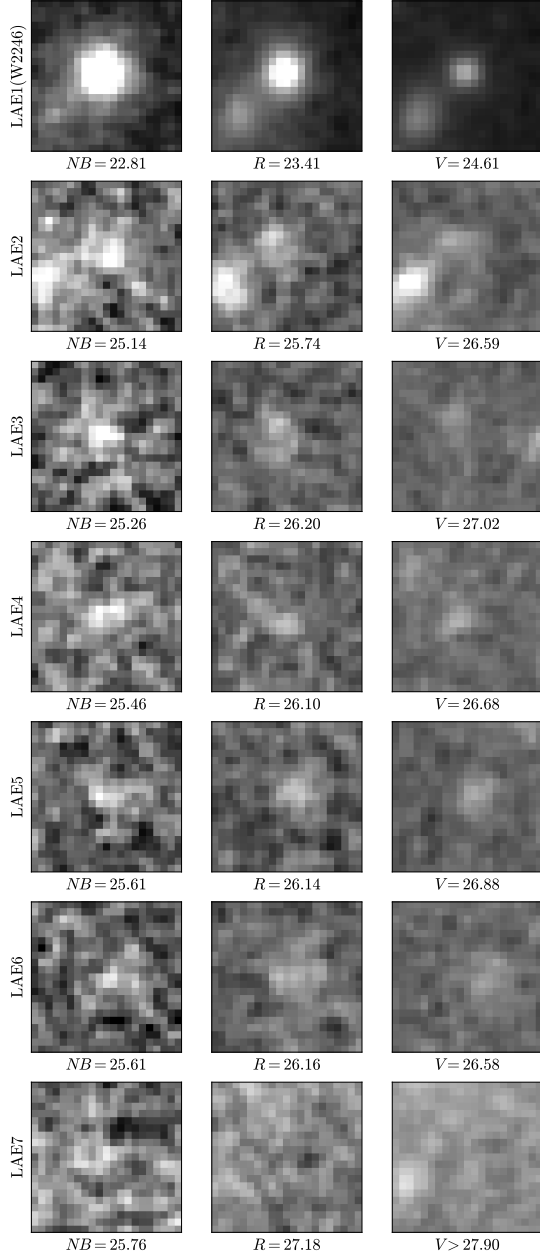| ID	R.A.	Decl.	NB_{tot}	$L_{Ly\alpha}$	SFR
	(J2000)	(J2000)	(AB mag)	$(\times 10^{42} \ erg \ s^{-1})$	$(M_\odot \ yr^{-1})$
LAE1(W2246)	341.53154167	-5.44305556	22.51	12.8	11.6
LAE2	341.52625438	-5.43420997	24.46	2.3	2.1
LAE3	341.48297707	-5.45017422	24.98	2.7	2.5
LAE4	341.52000180	-5.44773953	25.18	1.3	1.2
LAE5	341.47608618	-5.44077960	25.50	1.0	0.9
LAE6	341.57522991	-5.45600469	25.54	0.8	0.7
LAE7	341.50643274	-5.44953175	25.59	1.7	1.5

Figure 6. Postage stamps of LAE candidates in NB, R, and V bands. The size of each image is $5.3'' \times 5.3''$. For sources detected under the 2σ level in broadband, its magnitude in that band is denoted as $m > m_{lim,2\sigma}$.
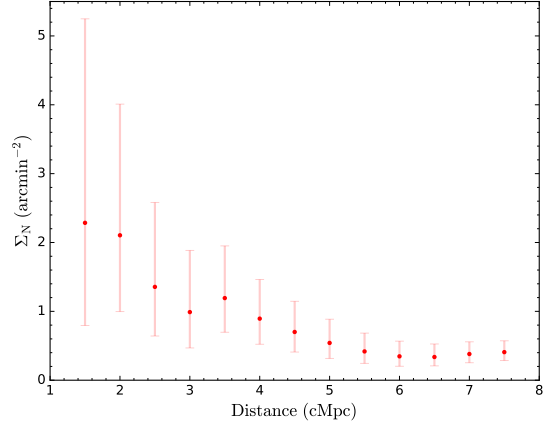

Figure 7. The surface density distribution of LAEs as a function of distance to Hot DOG W2246. The numbers of LAEs are corrected for completeness. Error bars are computed based on Gehrels (1986).

In order to study the environment of the Hot DOG W2246, we compare the number density of LAEs in W2246 field to values measured in blank fields. There are several studies focus on searching LAEs at redshift $z \approx 4.5$ in blank fields such as Boötes, Cetus, and CDFS fields (Dawson et al. 2007; Wang et al. 2009; Zheng et al. 2013), $Ly\alpha$ luminosity functions (LFs) are calculated based on those LAEs surveys. In particular, Zheng et al. (2013) derive a unified $Ly\alpha$ LF at $z \approx 4.5$ by combining all the LAEs found in Boötes, Cetus, and CDF-S fields. According to the FWHM of NB filter and the FOV of VLT/FORS2, the redshift volume V of our study can be derived. Then we can calculated the expected number of LAEs in the blank fields with the same volume V using the LFs. Notice that those $Ly\alpha$ LFs are built only using the spectroscopically confirmed LAEs, and the spectroscopic confirmation success rate $f_{\rm spec-confirm}$ for the LAE candidates (selecting through narrowband imaging) is about ~ 0.8 (Zheng et al. 2013). Therefore we assume $f_{\rm spec-confirm} = 0.8$ for our LAE candidates (except W2246 which has been spectroscopically confirmed) in this work. The number counts of LAEs are also performed completeness correction. We compare the number density of LAEs in W2246 field with the blank fields in different luminosity bin. The cumulative number densities of LAEs in the W2246 field and the blank fields as a function of $L_{Ly\alpha}$ are shown in Figure 8. We find that there is an overdensity of LAEs around W2246 compared to all the blank fields. The overdensity factor at $log[L_{Ly\alpha} \ (erg \ s^{-1})] > 42.0$ compared to Boötes field, Cetus field and combine fields are $2.1^{+1.0}_{-0.7}$, $1.9^{+0.9}_{-0.6}$, and $1.9^{+0.9}_{-0.6}$, respectively.

From Figure 7, we find the concentration of LAEs in the vicinity of Hot DOG W2246 and the size of the concentration region is small. The surface density of LAEs decreases rapidly with the increase of distance to Hot DOG W2246 and finally tends to stabilize at distance larger than 6 cMpc, which is 2.64 arcmin. Therefore, distance $r < 6$ cMpc may be a better scale to estimate environment of Hot DOG W2246 than using the whole W2246 field. As can be seen in Figure 8, if we only consider LAEs within 6 cMpc from Hot DOG W2246, the overdensity fatcor increases signifi-
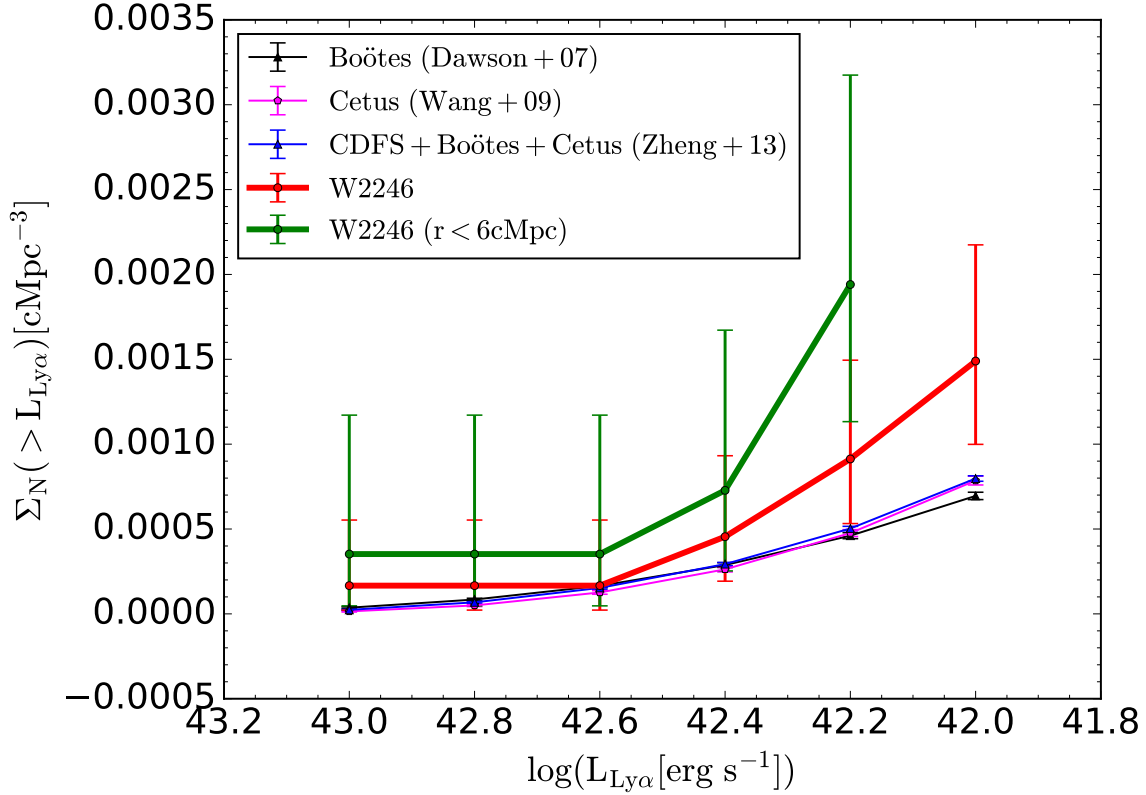
Figure 8. The cumulative number densities of LAEs in the W2246 field and the blank fields as a function of $L_{Ly\alpha}$. Error bars are based on Poisson statistics (Gehrels 1986).

cantly compared to the blank fields. The overdensity factor at $log[L_{Ly\alpha}\ (erg\ s^{-1})] > 42.2$ compared to Boötes field, Cetus field and combine fields are $4.2^{+2.7}_{-1.8}$, $4.1^{+2.6}_{-1.7}$, and $3.9^{+2.5}_{-1.6}$, respectively.

5. DISCUSSION

5.1. *Environments of Hot DOGs*

Hot DOGs have been found to reside in overdense environments by previous studies. Overdensities of submillimeter galaxies (SMGs) around Hot DOGs have been found using JCMT SCUBA2 850 μm observations. Compared to blank field SMGs survey, statistical overdensities of SMGs were revealed within 1.5 arcmin radius of Hot DOGs (Jones et al. 2014, 2017; Fan et al. 2017). Assef et al. (2015) statistically found overdensities of *Spitzer*-selected red galaxies around Hot DOGs within 1 arcmin radius compared to random pointing in blank field. For case studies, Luo et al. (2022) found an overdensity of DRGs around a Hot DOG at $z = 2.3$ using NIR selection and the overdensity factor was 2. Ginolfi et al. (2022) found an significant overdensity of LAEs around a $z = 3.6$ Hot DOG and the measured overdensity factor was 14 using the VLT/MUSE, which revealed that the Hot DOG lives in an extremely dense environment. For W2246, using ALMA observa-

tions, Diaz-Santos et al. (2018) found that W2246 is in a multiple merger system, with at least three spectroscopically confirmed companion galaxies within a few tens of kpc, indicating a kpc-scale overdensity around W2246. Zewdie et al. (2023) found an overdensity of LBGs around W2246, and the overdensity factor was 5.8 compared to the blank field. Considering projection effects in LBGs selection could dilute clustering signal, their result suggested that such a high overdensity factor can only be measured when W2246 resides in an extremely dense environment. Those studies suggested Hot DOGs may reside in overdense regions such as protoclusters and Hot DOGs could be the brightest cluster galaxies (BCGs) Assef et al. (2015); Zewdie et al. (2023).

In our work, we find that there is an overdensity of LAEs around W2246 compared to the blank fields, the overdensity factor is about 2 for the whole W2246 field and about 4 for region within 6 cMpc from Hot DOG W2246. Previous environmental studies of W2246 have found a kpc-scale overdensity around W2246 (Diaz-Santos et al. 2018) and an overdensity of LBGs around W2246 (Zewdie et al. 2023). Our study gives the direct evidence in Mpc scale that this most distant Hot DOG W2246 is in an overdense environment. The concentration of LAEs in the vicinity of Hot DOG W2246

suggests W2246 may reside in the densest region of the dense environment traced by itself. In addition, the impact of the shift of the observation window on our observed overdensity level needs to be considered. From the description of the narrowband filter information in Section 2 and the evolutionary track of an LAE in the left panel of Figure 4, we can find that when the redshift of an LAE is larger than the redshift of W2246, its Lyα emission line will move out of the narrowband filter wavelength coverage, which makes it undetectable in our observations. Therefore, if W2246 is at the center of the overdense region, only the side of the overdense region facing us can be observed using our data. As a result, the observed overdensity level is reduced, the intrinsic overdensity level will be higher than the value we calculated. Our result is consistent with previous environments studies of Hot DOGs, suggesting that Hot DOGs may be a good tracer for overdense regions. Galaxy overdensities regions such as protoclusters at high redshift are likely unvirialized (Chiang et al. 2013; Muldrew et al. 2015; Overzier 2016). Due to dense environments, mergers frequently occur during this period (Overzier 2016; Chapman et al. 2024). For Hot DOGs, high merger fraction has been found in a sample of Hot DOGs (Fan et al. 2016b). More kinematics studies of Hot DOGs suggested that Hot DOG stage could be sustained by minor mergers (Diaz-Santos et al. 2016, 2021; Ginolfi et al. 2022). Therefore, a scenario could be speculated that Hot DOG at the center of a protocluster merges with companion galaxies or tidal structures around, and experiences intense starbursts and rapid accretion, and final evolves to the BCG.

In Section 4.2 and Section 4.3, we suggest the region within 6 cMpc (2.64arcmin) distance from W2246 may be a better scale to estimate environment of Hot DOG W2246 than using the whole W2246 field. This suggests the size of the overdense region traced by W2246 such as protocluster could be small. Determining the scale of high-redshift protocluster is an important topic in cosmological simulations (Orsi et al. 2016; Izquierdo-Villalba et al. 2018), and since the number of high-redshift protocluster found so far is still very small, our qualitative analysis of the size of the overdense region at $z = 4.6$ could be useful for cosmological simulations.

The distribution of LAEs in Figure 1 seems to follow a filamentary-like orientation. Cosmological simulations predict that galaxy formation preferentially occurs along large-scale filamentary structures in the early universe. Filamentary structures are elongated and tens of Mpc in length. Protoclusters lie at the intersection of filaments in the cosmic web (Boylan-Kolchin et al. 2009; Codis et al. 2012; Laigle et al. 2015; Overzier 2016; Kraljic et al. 2018; Kuchner et al. 2020). In addition, Zheng et al. (2021) and Shi et al. (2021) found that the protocluster BOSS1542 at $z = 2.24$ shows a very extended filamentary structure over the scale of 23.4 cMpc. The environment study of the Hot DOG at $z = 3.6$ (Ginolfi et al. 2022) mentioned above also find LAEs appear to be aligned along the common orientation and shows filamentary structures. Similar structures have been found in a protocluster at $z = 2.84$ (Kikuta et al. 2019) and a protocluster at $z = 3.09$ (Umehata et al. 2019), suggesting filamentary structure may be a general feature of protoclusters in the early universe. Combining the results of previous theoretical simulations and observational studies, we potentially suggest that the distribution of LAEs in Figure 1 may be a filamentary structure.

6. SUMMARY AND CONCLUSION

In this work, we use VLT/FORS2 narrowband and broadband images to study the environment of the Hot DOG W2246 at $z = 4.6$ on Mpc scale. We search LAEs in W2246 field using color selection criteria. We find that there is an overdensity of LAEs in W2246 field compared with the blank fields. This is the direct evidence in Mpc scale that this most distant Hot DOG is in a overdense environment. Our result is consistent with previous environments studies of Hot DOGs, indicating that the environments of Hot DOGs are overdense. The overdense environment of Hot DOGs relates to merger origin of Hot DOGs, suggesting the growth of Hot DOGs by merging may happen in unvirialized overdense environments such as protoclusters.

Facilities: VLT(FORS2)

REFERENCES

Appenzeller, I., & Rupprecht, G. 1992, The Messenger, 67, 18

Assef, R. J., Eisenhardt, P. R. M., Stern, D., et al. 2015, ApJ, 804, 27, doi: 10.1088/0004-637X/804/1/27

Bertin, E., & Arnouts, S. 1996, A&AS, 117, 393, doi: 10.1051/aas:1996164

Bertin, E., Mellier, Y., Radovich, M., et al. 2002, in Astronomical Society of the Pacific Conference Series, Vol. 281, Astronomical Data Analysis Software and Systems XI, ed. D. A. Bohlender, D. Durand, & T. H. Handley, 228

Boylan-Kolchin, M., Springel, V., White, S. D. M., Jenkins, A., & Lemson, G. 2009, MNRAS, 398, 1150, doi: 10.1111/j.1365-2966.2009.15191.x

Cai, Z., Fan, X., Bian, F., et al. 2017, ApJ, 839, 131, doi: 10.3847/1538-4357/aa6a1a

Chapman, S. C., Hill, R., Aravena, M., et al. 2024, ApJ, 961, 120, doi: 10.3847/1538-4357/ad0b77

Chiang, Y.-K., Overzier, R., & Gebhardt, K. 2013, ApJ, 779, 127, doi: 10.1088/0004-637X/779/2/127

Codis, S., Pichon, C., Devriendt, J., et al. 2012, MNRAS, 427, 3320, doi: 10.1111/j.1365-2966.2012.21636.x

Dawson, S., Rhoads, J. E., Malhotra, S., et al. 2007, ApJ, 671, 1227, doi: 10.1086/522908

Di Matteo, P., Bournaud, F., Martig, M., et al. 2008, A&A, 492, 31, doi: 10.1051/0004-6361:200809480

Diaz-Santos, T., Assef, R. J., Blain, A. W., et al. 2016, ApJL, 816, L6, doi: 10.3847/2041-8205/816/1/L6

—. 2018, Science, 362, 1034, doi: 10.1126/science.aap7605

Diaz-Santos, T., Assef, R. J., Eisenhardt, P. R. M., et al. 2021, A&A, 654, A37, doi: 10.1051/0004-6361/202140455

Eisenhardt, P. R. M., Wu, J., Tsai, C.-W., et al. 2012, ApJ, 755, 173, doi: 10.1088/0004-637X/755/2/173

Fan, L., Chen, W., An, T., et al. 2020, ApJL, 905, L32, doi: 10.3847/2041-8213/abcebf

Fan, L., Gao, Y., Knudsen, K. K., & Shu, X. 2018, ApJ, 854, 157, doi: 10.3847/1538-4357/aaaaae

Fan, L., Han, Y., Nikutta, R., Drouart, G., & Knudsen, K. K. 2016a, ApJ, 823, 107, doi: 10.3847/0004-637X/823/2/107

Fan, L., Jones, S. F., Han, Y., & Knudsen, K. K. 2017, PASP, 129, 124101, doi: 10.1088/1538-3873/aa8e91

Fan, L., Han, Y., Fang, G., et al. 2016b, ApJL, 822, L32, doi: 10.3847/2041-8205/822/2/L32

Fernández Aranda, R., Díaz Santos, T., Hatziminaoglou, E., et al. 2024, A&A, 682, A166, doi: 10.1051/0004-6361/202347869

Freudling, W., Romaniello, M., Bramich, D. M., et al. 2013, A&A, 559, A96, doi: 10.1051/0004-6361/201322494

García-Vergara, C., Hennawi, J. F., Barrientos, L. F., & Arrigoni Battaia, F. 2019, ApJ, 886, 79, doi: 10.3847/1538-4357/ab4d52

Gehrels, N. 1986, ApJ, 303, 336, doi: 10.1086/164079

Ginolfi, M., Piconcelli, E., Zappacosta, L., et al. 2022, Nature Communications, 13, 4574, doi: 10.1038/s41467-022-32297-x

Hamuy, M., Suntzeff, N. B., Heathcote, S. R., et al. 1994, PASP, 106, 566, doi: 10.1086/133417

Hamuy, M., Walker, A. R., Suntzeff, N. B., et al. 1992, PASP, 104, 533, doi: 10.1086/133028

Hopkins, P. F., Somerville, R. S., Hernquist, L., et al. 2006, ApJ, 652, 864, doi: 10.1086/508503

Hu, W., Wang, J., Zheng, Z.-Y., et al. 2019, ApJ, 886, 90, doi: 10.3847/1538-4357/ab4cf4

Hu, W., Wang, J., Infante, L., et al. 2021, Nature Astronomy, 5, 485, doi: 10.1038/s41550-020-01291-y

Inoue, A. K., Shimizu, I., Iwata, I., & Tanaka, M. 2014, MNRAS, 442, 1805, doi: 10.1093/mnras/stu936

Izquierdo-Villalba, D., Orsi, Á. A., Bonoli, S., et al. 2018, MNRAS, 480, 1340, doi: 10.1093/mnras/sty1941

Jones, S. F., Blain, A. W., Stern, D., et al. 2014, MNRAS, 443, 146, doi: 10.1093/mnras/stu1157

Jones, S. F., Blain, A. W., Assef, R. J., et al. 2017, MNRAS, 469, 4565, doi: 10.1093/mnras/stx1141

Kikuta, S., Imanishi, M., Matsuoka, Y., et al. 2017, ApJ, 841, 128, doi: 10.3847/1538-4357/aa72f0

Kikuta, S., Matsuda, Y., Cen, R., et al. 2019, PASJ, 71, L2, doi: 10.1093/pasj/psz055

Komatsu, E., Smith, K. M., Dunkley, J., et al. 2011, ApJS, 192, 18, doi: 10.1088/0067-0049/192/2/18

Kraljic, K., Arnouts, S., Pichon, C., et al. 2018, MNRAS, 474, 547, doi: 10.1093/mnras/stx2638

Kuchner, U., Aragón-Salamanca, A., Pearce, F. R., et al. 2020, MNRAS, 494, 5473, doi: 10.1093/mnras/staa1083

Laigle, C., Pichon, C., Codis, S., et al. 2015, MNRAS, 446, 2744, doi: 10.1093/mnras/stu2289

Liang, Y., Kashikawa, N., Cai, Z., et al. 2021, ApJ, 907, 3, doi: 10.3847/1538-4357/abcd93

Luo, Y., Fan, L., Zou, H., et al. 2022, ApJ, 935, 80, doi: 10.3847/1538-4357/ac8162

Mazzucchelli, C., Bañados, E., Decarli, R., et al. 2017, ApJ, 834, 83, doi: 10.3847/1538-4357/834/1/83

Muldrew, S. I., Hatch, N. A., & Cooke, E. A. 2015, MNRAS, 452, 2528, doi: 10.1093/mnras/stv1449

Orsi, Á. A., Fanidakis, N., Lacey, C. G., & Baugh, C. M. 2016, MNRAS, 456, 3827, doi: 10.1093/mnras/stv2919

Ouchi, M., Ono, Y., & Shibuya, T. 2020, ARA&A, 58, 617, doi: 10.1146/annurev-astro-032620-021859

Ouchi, M., Shimasaku, K., Akiyama, M., et al. 2008, ApJS, 176, 301, doi: 10.1086/527673

Overzier, R. A. 2016, A&A Rv, 24, 14, doi: 10.1007/s00159-016-0100-3

Piconcelli, E., Vignali, C., Bianchi, S., et al. 2015, A&A, 574, L9, doi: 10.1051/0004-6361/201425324

Pirzkal, N., Rothberg, B., Ly, C., et al. 2013, ApJ, 772, 48, doi: 10.1088/0004-637X/772/1/48

Polletta, M., Tajer, M., Maraschi, L., et al. 2007, ApJ, 663, 81, doi: 10.1086/518113

Schlafly, E. F., & Finkbeiner, D. P. 2011, ApJ, 737, 103, doi: 10.1088/0004-637X/737/2/103

Shi, D. D., Cai, Z., Fan, X., et al. 2021, ApJ, 915, 32, doi: 10.3847/1538-4357/abfec0

Stern, D., Lansbury, G. B., Assef, R. J., et al. 2014, ApJ, 794, 102, doi: 10.1088/0004-637X/794/2/102

Stetson, P. B. 2000, PASP, 112, 925, doi: 10.1086/316595

Sun, W., Fan, L., Han, Y., et al. 2024, ApJ, 964, 95, doi: 10.3847/1538-4357/ad22e3

Tsai, C.-W., Eisenhardt, P. R. M., Wu, J., et al. 2015, ApJ, 805, 90, doi: 10.1088/0004-637X/805/2/90

Tsai, C.-W., Eisenhardt, P. R. M., Jun, H. D., et al. 2018, ApJ, 868, 15, doi: 10.3847/1538-4357/aae698

Turnshek, D. A., Bohlin, R. C., Williamson, R. L., I., et al. 1990, AJ, 99, 1243, doi: 10.1086/115413

Umehata, H., Fumagalli, M., Smail, I., et al. 2019, Science, 366, 97, doi: 10.1126/science.aaw5949

Venemans, B. P., Kurk, J. D., Miley, G. K., et al. 2002, ApJL, 569, L11, doi: 10.1086/340563

Venemans, B. P., Röttgering, H. J. A., Miley, G. K., et al. 2005, A&A, 431, 793, doi: 10.1051/0004-6361:20042038

—. 2007, A&A, 461, 823, doi: 10.1051/0004-6361:20053941

Wang, J.-X., Malhotra, S., Rhoads, J. E., Zhang, H.-T., & Finkelstein, S. L. 2009, ApJ, 706, 762, doi: 10.1088/0004-637X/706/1/762

Wu, J., Tsai, C.-W., Sayers, J., et al. 2012, ApJ, 756, 96, doi: 10.1088/0004-637X/756/1/96

Zewdie, D., Assef, R. J., Mazzucchelli, C., et al. 2023, A&A, 677, A54, doi: 10.1051/0004-6361/202346695

Zheng, X. Z., Cai, Z., An, F. X., Fan, X., & Shi, D. D. 2021, MNRAS, 500, 4354, doi: 10.1093/mnras/staa2882

Zheng, Z.-Y., Finkelstein, S. L., Finkelstein, K., et al. 2013, MNRAS, 431, 3589, doi: 10.1093/mnras/stt440

Zheng, Z.-Y., Wang, J., Rhoads, J., et al. 2017, ApJL, 842, L22, doi: 10.3847/2041-8213/aa794f